Environmental Science and Pollution Research (2024) 31:10838–10852
https://doi.org/10.1007/s11356-023-31754-4

RESEARCH ARTICLE

Critical role of zero-valent iron in the efficient activation of H_2O_2 for 4-CP degradation by bimetallic peroxidase-like

Xinxin Lv[1,2] · Huilai Liu[1,2] · Zhihao Li[1,2] · Minshu Cui[1] · Kangping Cui[1] · Zhi Guo[1] · Zhengliang Dai[3] · Bei Wang[3] · Xing Chen[1,2]

Received: 4 October 2023 / Accepted: 23 December 2023 / Published online: 12 January 2024

Abstract

Peroxidase-like based on double transition metals have higher catalytic activity and are considered to have great potential for application in the field of pollutant degradation. First, in this paper, a novel Fe^0-doped three-dimensional porous Fe^0@FeMn-NC-like peroxidase was synthesized by a simple one-step thermal reduction method. The doping of manganese was able to reduce part of the iron in Fe-Mn binary oxides to Fe^0 at high temperatures. In addition, Fe^0@FeMn-NC has excellent peroxidase-like mimetic activity, and thus, it was used for the rapid degradation of p-chlorophenol (4-CP). During the degradation process, Fe^0 was able to rapidly replenish the constantly depleted Fe^{2+} in the reaction system and brought in a large number of additional electrons. The ineffective decomposition of H_2O_2 due to the use of H_2O_2 as an electron donor in the reduction reactions from Fe^{3+} to Fe^{2+} and from Mn^{3+} to Mn^{2+} was avoided. Finally, based on the experimental results of LC-MS and combined with theoretical calculations, the degradation process of 4-CP was rationally analyzed, in which the intermediates were mainly p-chloro-catechol, p-chloro resorcinol, and p-benzoquinone. Fe^0@FeMn-NC nano-enzymes have excellent catalytic activity as well as structural stability and perform well in the treatment of simulated wastewater containing a variety of phenolic pollutants as well as real chemical wastewater. It provides some insights and methods for the application of peroxidase-like enzymes in the degradation of organic pollutants.

Keywords ZVI · Fe-Mn bimetal · POD-like activity · H_2O_2 activation · p-Chlorophenol (4-CP) degradation

Introduction

Phenolic pollutants are widely present in industrial processes such as pharmaceuticals, paper, printing, and dyeing (Zhang et al. 2007). Incompletely treated industrial wastewater often contains phenolics, which have serious effects on human and animal physiology when discharged into the environment and can accumulate in organisms, with the risk of carcinogenicity and teratogenicity (Hu et al. 2021; Villaluz et al. 2019). Among the monochlorophenols, p-chlorophenol (4-CP) is the most toxic (Czaplicka 2004), and chlorophenol-containing wastewater must be treated before it is discharged into the environment. Therefore, it is necessary to find an effective method to remove phenolics from wastewater.

Green chemistry technologies using nano-enzymes as catalysts are receiving more and more attention compared to traditional physical and chemical treatment methods (Liu et al. 2023b; Mishra et al. 2022; Wang and Chen 2020). Among them, peroxidase-like enzymes, which can catalyze the activated decomposition of H_2O_2 to produce hydroxyl radicals (•OH) with stronger oxidizing ability, have been intensively studied in the field of advanced oxygenation of organic pollutants (Chen et al. 2020; Tang et al. 2023; Yang et al. 2020). As an effective peroxidase-like mimic, metal-based nanomaterials have been successfully applied to

Responsible Editor: George Z. Kyzas

✉ Xing Chen
xingchen@hfut.edu.cn

[1] Key Laboratory of Nanominerals and Pollution Control of Higher Education Institutes, School of Resources and Environmental Engineering, Hefei University of Technology, Hefei 230009, People's Republic of China

[2] Key Lab of Aerospace Structural Parts Forming Technology and Equipment of Anhui Province, Institute of Industry and Equipment Technology, Hefei University of Technology, Hefei 230009, People's Republic of China

[3] Anqing Changhong Chemical Co., Ltd., Anqing 246002, People's Republic of China

remove chlorophenols from laboratory synthetic wastewaters and real industrial wastewaters due to their excellent electron transfer ability (Tang et al. 2023). For example, Xin et al. prepared AA-NiMn-CLDHs@HNTs-Ag nanomotors by assembling AgNPs and NiMn-CLDH nanosheets inside and outside the lumen of natural halloysite nanotubes (HNTs) using a layer-by-layer self-assembly technique, which was able to degrade 95.63% of phenol within 90 min (Xing et al. 2022). Magnetic material Au@Ni/rGO with a size less than 8 nm and core-shell nanostructure was successfully synthesized and exhibited peroxidase-like activity, exhibiting excellent performance in the photodegradation behavior of phenol, 2-chlorophenol, and 2-nitrophenol (Darabdhara and Das 2019). However, the cost of precious metals and the scarcity of the material are also difficulties that have to be faced at the material preparation stage. Iron-based materials, as a peroxidase-like, have received increasing attention from researchers due to their environmental-friendly properties and low cost (Huang et al. 2023; Jiang et al. 2021; Jiao et al. 2020; Wan et al. 2022). Among them, zero-valent iron and iron oxides have been shown to possess peroxidase-like activity, while Fe_3O_4 is an ideal feedstock for catalysts due to its magnetic properties facilitating material recycling (Baye et al. 2023; Liu et al. 2022). However, the use of iron-based nano-enzymes alone comes with unavoidable drawbacks such as low Fe^{2+}/Fe^{3+} recovery and high ion leaching. Therefore, it is crucial to improve the stability of iron-based materials and their catalytic properties.

Manganese, as a widespread element in the environment, has a wide variety of valence states and excellent redox properties (Cai et al. 2021; Du et al. 2020; He et al. 2022; Hu et al. 2017). Some studies have shown that Mn^{2+}, Mn^{3+}, and Mn^{4+} can exhibit peroxidase mimetic activities (Ding et al. 2021; Lv et al. 2023; Meng et al. 2020). However, manganese-based nano-enzymes are often difficult to recover, which limits their wide application in water pollution treatment. Therefore, iron-manganese bimetallic nano-catalytic materials can effectively solve the problems of material recycling as well as material stability, achieving the best of both worlds. Due to the synergistic effect between Fe-Mn, Fe-Mn bimetallic nano-enzymes tend to exhibit stronger catalytic performance than the corresponding monometallic nano-enzymes (Huang et al. 2022; Qu et al. 2021; Wang et al. 2019). This has been widely applied in the field of pollutant degradation and detection and sensing (Liu et al. 2023a; Mao et al. 2023; Martins et al. 2023; Sun et al. 2021; Zhang et al. 2022). For example, Liang et al. showed that redox cycling between Fe^{3+}/Fe^{2+} and Mn^{3+}/Mn^{2+} can promote the generation of free radicals, thus showing excellent performance in the degradation of tetracycline (Liang et al. 2023); Liu et al. found that Mn-amplified Fe-N nano-enzymes have more excellent peroxidase-like activity, which is attributed to the strong electron transfer properties of Fe and Mn, which can accelerate the decomposition of H_2O_2 to produce more •OH (Liu et al. 2023a). For carbon-based materials, high-temperature pyrolysis favors the formation of a large number of carbon vacancies, which can significantly accelerate the redox step (Wei et al. 2023). In addition, bimetallic nano-enzymes were found to have d-orbital coupling features that contribute to the lowering of electron transfer energy barriers in redox (Feng et al. 2023). However, polymetallic nano-enzymes are still poorly studied, and efforts are still needed to fill this research gap.

In this work, to further improve the catalytic activity as well as stability of the nano-enzyme, we employed a simple high-temperature pyrolysis reduction method to synthesize a novel Fe^0-doped three-dimensional porous FeMn-NC nano-enzyme for the catalytic degradation of 4-CP (Scheme 1a). Among them, Fe^0@FeMn-NC exhibited excellent peroxidase-like (POD-like) activity with high H_2O_2 affinity and catalytic efficiency. Moreover, the presence of Fe^0 could effectively replenish the Fe^{2+} consumed in the reaction, avoiding the ineffective decomposition of H_2O_2 and enabling more hydroxyl radicals (•OH), superoxide radicals ($•O_2^-$), and singlet oxygen ($^1O_2$) to be used for the degradation of pollutants (Scheme 1b). Fe^0@FeMn-NC nano-enzyme have excellent catalytic activity and structural stability and are effective in treating both simulated wastewater containing various phenolic pollutants as well as real chemical wastewater.

Materials and methods

Materials and drugs

D(+)-glucosamine hydrochloride, dicyandiamide, 3,3′,5,5′–tetramethylbenzidine (TMB), and $ZnCl_2$ were purchased from Shanghai Maclin Biochemical Co., Ltd. $FeCl_3•6H_2O$, $MnCl_2$, H_2O_2 (30 wt%), glacial acetic acid, anhydrous sodium acetate, anhydrous ethanol, tert-butanol (TBA), p-benzoquinone (PBQ), furfuryl alcohol (FFA), p-chlorophenol (4-CP), p-nitrophenol (4-NP), phenol, paracetamol (PCM), bisphenol A (BPA), hydrochloric acid, NaOH, and 2,2,6,6-tetramethylpiperidine (TEMP) were purchased from Sinophenol Chemical Reagents Co., Ltd. 5,5-Dimethyl-1-pyrroline N-oxide (DMPO) was purchased from Dojindo Laboratories. All chemicals are used as received without further purification. All aqueous solutions were prepared with deionized water (18.25 MΩ·cm, microporous).

Instruments

High-resolution field emission scanning electron microscopy (FESEM, Regulus 8230, Japan) was used to record

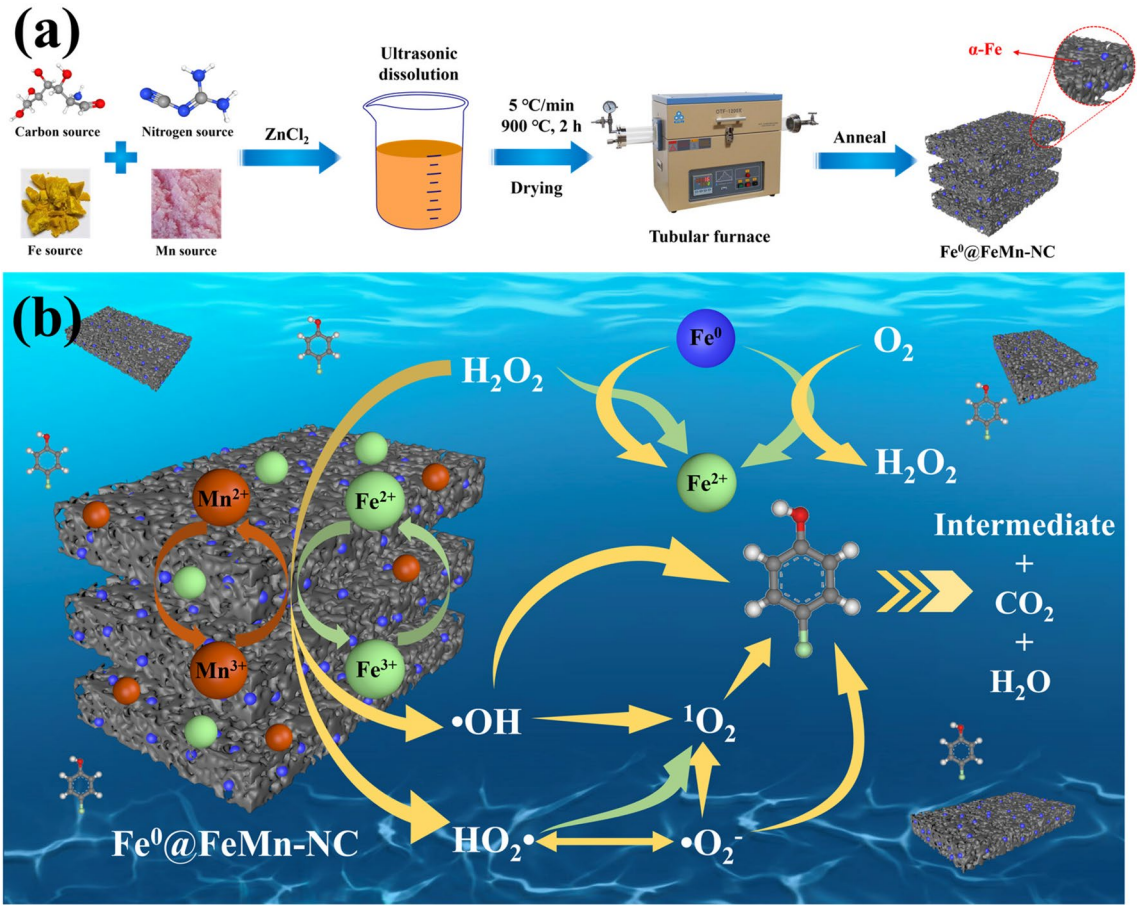

Scheme 1 Schematic flow diagram of the preparation of Fe^0@FeMn-NC nano-enzymes (**a**) and their application in the degradation of 4-CP by activated H_2O_2 (**b**)

scanning electron microscopy images. Transmission electron microscopy (TEM) imaging was performed on a JEM-2100F microscope at an acceleration voltage of 200 kV (JEOL, Japan). The specific surface area and pore structure of the materials were measured by the AutosorB-IQ3 N_2 adsorption-desorption instrument (Kantha, USA). X-ray photoelectron spectroscopy (XPS) spectra were collected by an ESCALAB250Xi XPS microscope (Thermo, USA). UV-visible absorption spectra were collected by UV-visible spectrophotometer (SHIMADZU, Japan). Raman analysis was performed on a LabRAM HR Evolution (France) spectrometer with an argon ion laser (532 nm) as the excitation source. The XRD patterns of the materials were recorded by an X-ray diffractometer (Rigaku D/MAX2500VL/PC, Japan). The concentration of metal ions leached in solution was determined by atomic absorption spectrometer (Perkin Elmer AA800, USA). Electron paramagnetic resonance (EPR) measurements were carried out on a JES-FA200 spectrometer (JEOL, Japan). The TOC removal rate was measured by Multi N/C 3100 TOC analyzer (Jena, Germany). The intermediates in the reaction process were analyzed by liquid chromatography-four-stage electrostatic field orbital trap mass spectrometry (LC-MS, Thermo, USA).

Synthesis of Fe^0@FeMn-NCnanocomposite catalysts

The Fe^0@FeMn-NC nanocatalysts required for the experiments were synthesized by a one-step pyrolysis method. Firstly, D(+)-glucosamine hydrochloride and dicyandiamide were used as carbon and nitrogen sources, $ZnCl_2$ as a pore-forming agent, and $FeCl_3$-$6H_2O$ and $MnCl_2$ as iron and manganese sources, respectively, which were dissolved into a certain amount of deionized water in a molar ratio of 10:10:2:1:1, respectively, by ultrasonic dissolution. After drying the above solution, the solid obtained was transferred to a tube furnace and heated up to 900 °C at a heating rate of 5 °C/min in an atmosphere of N_2. Holding time was 2 h, and then annealed to obtain Fe^0@FeMn-NC. Finally, NC-900, Fe-NC, and Mn-NC were prepared by the same scheme described above under the conditions of no metal doping and Fe/Mn ratios of 2:0, 0:2, respectively.

Peroxidase activity measurement

To study the peroxidase-like activity of FeMn-NC nano-enzymes, TMB was selected as the substrate for colorimetric assay. Fe^0@FeMn-NC nano-enzymes (40 mg/L) were added to HAc-NaAc buffer solution (pH = 4) containing TMB (0.3 mM) and H_2O_2 (10 mM). After incubation at room temperature (25 °C) for 5 min to produce the corresponding blue color reaction, 1 mL of the solution was removed from the tube and filtered through a microporous filter (0.45 μm) and transferred to a UV-vis spectrophotometer to measure the absorbance value at 652 nm.

In the steady-state kinetic experiments, we fixed the TMB concentration at 0.3 mM and performed kinetic analysis of different concentrations of H_2O_2 by varying the H_2O_2 concentration and recording the absorbance at 652 nm at selected time intervals in a scanning kinetic mode. Apparent kinetic parameters (K_m and V_{max}) were obtained through typical Miltonian equation and double-reciprocal equation diagrams (Zhang et al. 2021), as shown in Eq. (1):

$$\frac{1}{V}=\left(\frac{K_m}{V_{max}}\right)\frac{1}{[S]}+\frac{1}{V_{max}} \quad (1)$$

where V represents the initial reaction rate, V_{max} represents the maximum reaction rate, [S] represents the substrate concentration, and K_m represents the Michaelis–Menten constant.

4-CP adsorption and degradation experiments

The catalytic performance of the Fe^0@FeMn-NC nano-enzyme catalyst was evaluated based on the degradation efficiency of 4-CP in the presence of H_2O_2. The effects of several important parameters of 4-CP degradation such as H_2O_2 concentration, initial pH, and catalyst dosing on the 4-CP degradation efficiency were explored. The experimental procedure was as follows: 50 mL of mixture containing catalyst (40 mg/L) and 4-CP (100 mg/L) was added into a 50-mL conical flask, pH was adjusted and stirred continuously for 30 min to reach the adsorption equilibrium, and then, a certain concentration of H_2O_2 was added with continuous stirring. One milliliter of liquid was removed from the reaction solution at 0, 2, 5, 10, and 30 min, respectively, and filtered through a 0.45-μm membrane to remove the catalyst, and an excess of anhydrous methanol was added to quench the unreacted radicals to inhibit further reaction. Finally, the obtained samples were analyzed by high performance liquid chromatography (HPLC, LC-20A, Shimadzu, Japan) for the determination of 4-CP. The catalysts were collected by filtration at the end of each run and then washed at least five times with ethanol and deionized water, dried, and reserved for the next cycle of experiments. Subsequent degradation experiments with 4-NP, BPA, PCM, Phenol, and actual wastewater were conducted using the same methodology as described above.

DFT calculations

All calculations are based on Materials Studio DMol^3 version 2020 (Delley 1990, 2000). Geometry optimization and energy minimization of the compounds were carried out using the Generalized Gradient Approximation (GGA) and the Perdew-Burke-Ernzerhof (PBE) exchange function (Perdew et al. 1996). The cutoff energy of the plane-wave basis set is 380 eV. In the geometric optimization, the energy convergence criterion of the system is set to 1×10^{-5} eV, with a force of less than 0.03 eV/Å per atom. For the 4-CP degradation process, we use Linear Synchronous Transition/Quadratic Synchronous Transition (LST/QST) for the transition state search and verify whether the transition state has only one imaginary frequency by frequency analysis. Then, transition state confirmation is performed based on the Nudged Elastic Band (NEB) method.

Results and discussion

Physical characterization of the material

XRD characterization was performed to explore the crystalline phase of the nano-enzymes. As shown in Fig. 1a, all materials exhibited characteristic peaks (broad diffraction peaks at 20–25°) similar to the graphitized carbon nitride of NC-900. The diffraction peaks appearing at 35.4°, 41.2°, and 59.6° are attributed to the (111), (200), and (220) crystal planes of the Fe-Mn oxides, respectively. In Fe-NC and Mn-NC there are only characteristic peaks of Fe-Mn oxides. When Fe-Mn is doped simultaneously, new diffraction peaks appear at 44.7°,65.2°, and 82.5°, corresponding to the (110), (200), and (211) crystal planes of α-Fe, respectively (Gong et al. 2021). This is due to the fact that Fe in Fe oxides can be stripped out and reduced to zero-valent Fe by Mn under high temperature environment (Xu et al. 2023b). Figure 1b shows the Raman spectra of NC-900, Fe-NC, Mn-NC, and Fe^0@FeMn-NC, which can reflect their defective information. The D peak (1350 cm^{-1}) corresponds to the sp^3 hybridization of carbon atoms, and the G peak (1580 cm^{-1}) is due to the intra-structural scaling of the sp^2 hybridization of carbon atoms (Ananthoju et al. 2019). All materials have broad D-band peaks, indicating the presence of abundant defects in the carbon matrix, to play an important role in improving the catalytic activity of the catalysts. In addition, the value of I_D/I_G decreases significantly with the doping of Fe-Mn; this is due to the emergence of Fe-Mn crystallization, which

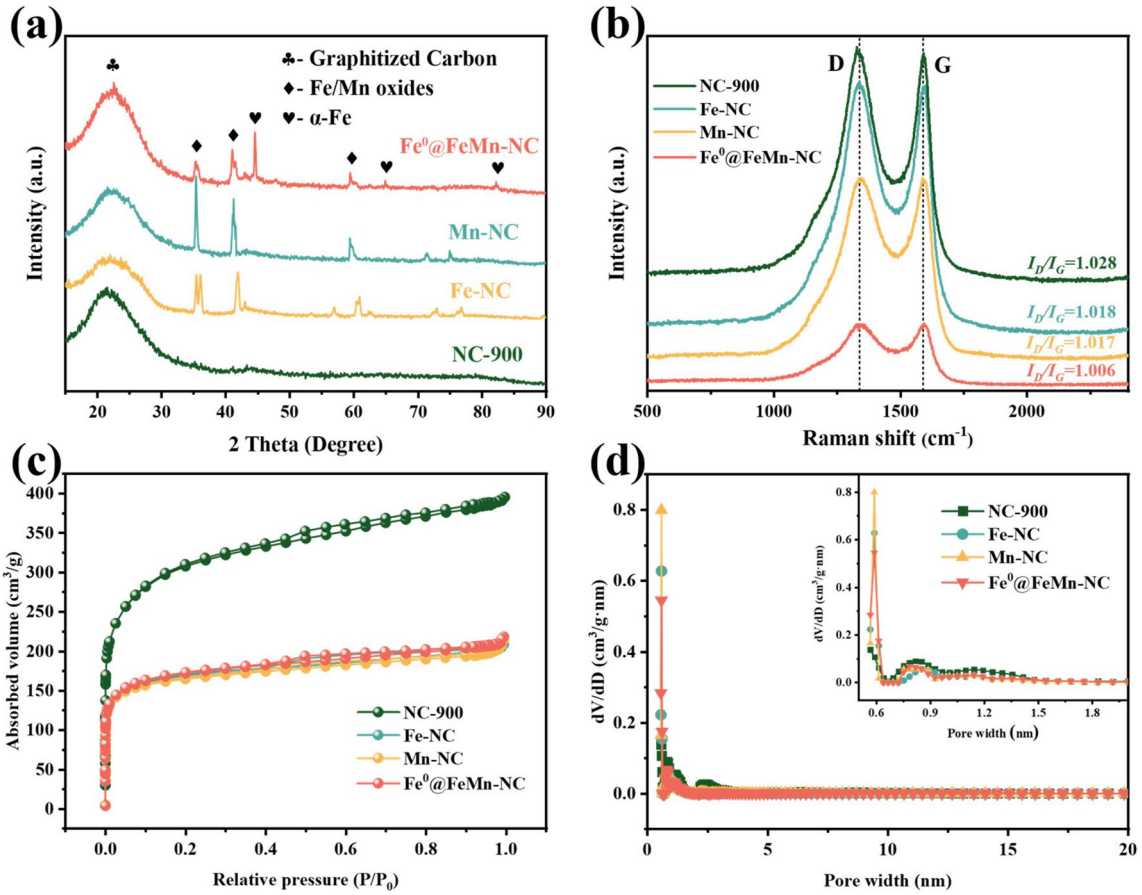

Fig. 1 The XRD patterns (**a**), Raman spectra (**b**), N_2 adsorption/desorption isotherms (**c**), and corresponding DFT pore-size distribution (**d**) of NC-900, Fe-NC, Mn-NC, and Fe^0@FeMn-NC

makes the catalyst gradually tend to be ordered. The porous carbon layer in Fe^0@FeMn-NC plays an important role for electron transfer within the system. As shown in Fig. 1c, all the samples exhibit a typical type I adsorption isotherm for microporous materials, associated with the presence of a large number of microporous structures, where intra-microporous adsorption occurs in the low-pressure region, leading to a sharp increase in adsorption, whereas a slow rise in the adsorption plateau suggests that there is a trace amount of hollow and microporous structures in the material (Lai et al. 2016; Liang et al. 2014). The hysteresis loop appears in the region of higher relative pressure, showing a typical type IV adsorption isotherm, which was shown to be related to the presence of meso- and microporous structures in the carbon structure (Zhang et al. 2018). The pore size distribution and specific surface area of the nanocatalysts were calculated by the DFT method, and the results are shown in Fig. 1d and Table S1. The pore sizes are mainly distributed in the range of 0.5–5 nm, belonging to the typical micro-mesoporous materials, and are mainly dominated by micropores distributed below 2 nm. This phenomenon suggests that Fe^0@FeMn-NC has formed a layered pore structure that is favorable for increasing the reaction sites and thus enhancing the reaction activity. By comparing the enlarged pore size distribution (inset in Fig. 1d) and the specific surface area (Table S1), it can be seen that the number of micropores and the specific surface area appeared to decrease after loading the metal, which was attributed to the metal particles having a certain blocking effect on the micropores of the material.

Figure S1 shows the SEM images of NC-900, Fe-NC, Mn-NC, and Fe^0@FeMn-NC, which exhibit irregular porous features. Similar to NC-900, they all have a large number of graded porous structures, which suggests that Fe/Mn doping does not affect the macrostructure of carbon nitride (Wang and Nan 2020). A granular structure was clearly observed from the TEM images of Fe^0@FeMn-NC (Fig. 2a, b), which could be the doped Fe and Mn species (Xu et al. 2023a). The HR-TEM images showed (Fig. 2c, d) that the interfacial spacing of the carbon matrix was 0.34 nm, suggesting that a large amount of graphitized carbon was formed in Fe^0@FeMn-NC (He et al. 2024). The 0.22-nm and 0.25-nm interfacial spacing is attributed to the (200) and (111) crystal faces of the Fe–Mn oxides. In addition, the (110)

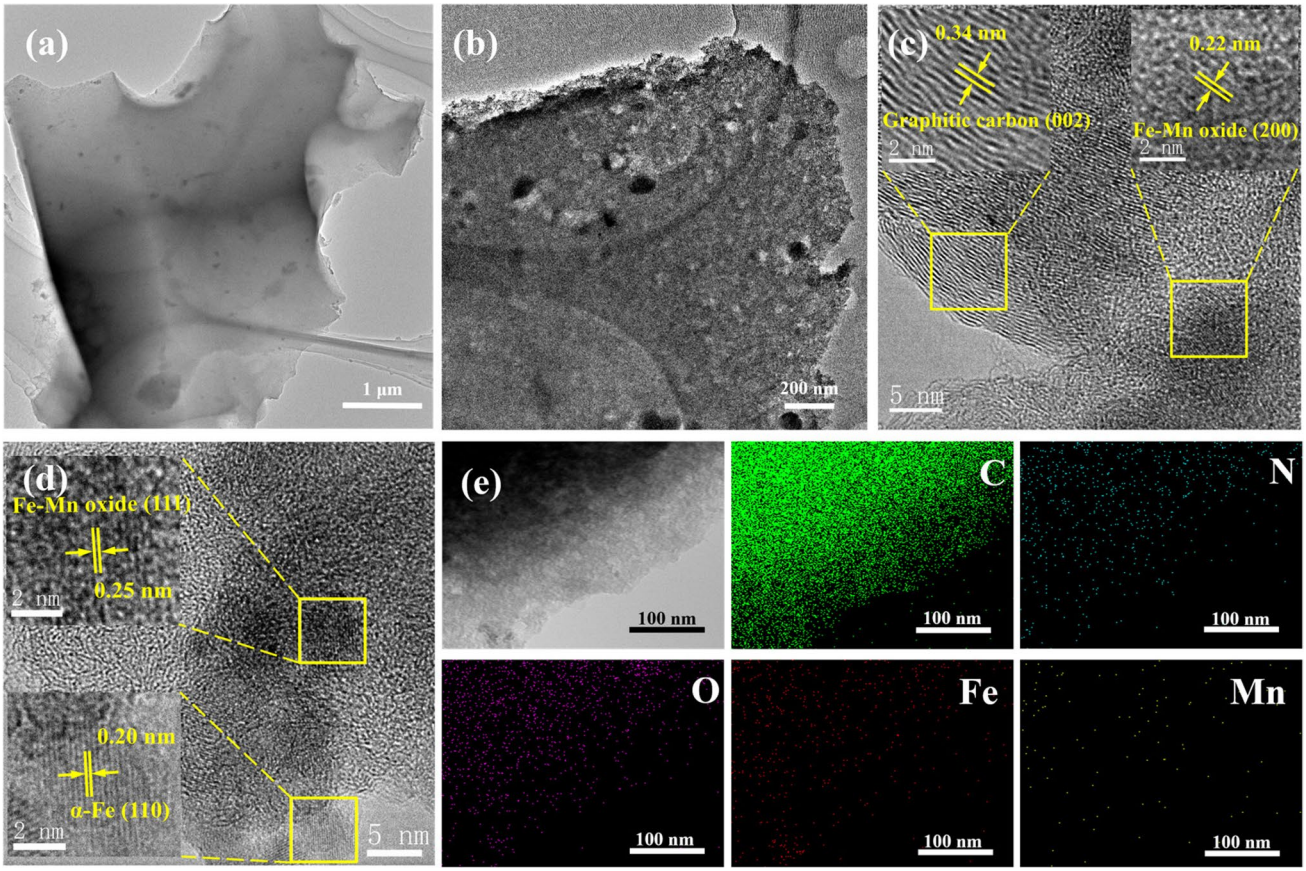

Fig. 2 The TEM (**a**, **b**), HR-TEM (**c**, **d**), and EDS elemental mapping images (**e**) of Fe^0@FeMn-NC

crystal face of α-Fe (with an interfacial spacing of 0.20 nm) can be clearly seen (Xu et al. 2023b). The energy dispersive X-ray spectroscopy (EDS) mapping images in Fig. 2e show a homogeneous distribution of the elements C, N, O, Fe, and Mn on Fe^0@FeMn-NC. This is in agreement with our results described in XRD, indicating that Fe^0 was successfully synthesized on a carbon matrix where Fe-Mn oxides coexist.

The elemental composition and state of Fe^0@FeMn-NC were determined through further characterization by XPS. Significant C, N, and O signals, as well as weak Fe and Mn signals, can be observed in the XPS gross spectrum of Fe^0@FeMn-NC (Fig. S2a), which is because the amounts of Fe and Mn are trace compared to carbon and nitrogen during the material synthesis process. Among them, C 1 s was able to be indexed as C-C (284.8 eV), C-N (286.0 eV), and C-O (288.1 eV) structures (Fig. S2b) (He et al. 2023; Zhu et al. 2018). In its high-resolution N 1 s XPS spectra (Fig. S2c), four different types of N, Pyridinic-N (398.5 eV), Graphitic-N (400.9 eV), Oxidized-N (402.7 eV), and M-N_X (399.7 eV), were observed, demonstrating that the material forms abundant Fe-N_X and Mn-N_X, which can provide a large number of active sites for the catalytic reaction to proceed (Deng et al. 2017). In the O 1 s profile (Fig. S2d), it was possible to quickly fit three distinct characteristic peaks indexed as M–O (530.2 eV), M–O-C (531.8 eV), and C-O (533.4 eV), respectively (Duan et al. 2022). The Fe 2p pattern (Fig. 3a) with distinct characteristic peaks of Fe^0 (705.4 eV), Fe^{2+} (710.6 eV and 723.9 eV), and Fe^{3+} (713.8 eV and 726.9 eV) reconfirms the successful synthesis of zero-valent iron in Fe^0@FeMn-NC, which would be more favorable for the activation of peroxide (Lin et al. 2017; Yamashita and Hayes 2008). The spectrum of Mn 2p is shown in Fig. 3b, which can be back-convoluted to the characteristic peaks of Mn^{2+} (640.2 eV and 652.4 eV), Mn^{3+} (641.4 eV and 653.7 eV), and Mn^{4+} (643.0 eV and 655.3 eV) (He et al. 2024). All these results are in agreement with the conclusions obtained in the previous characterization.

Peroxidase activity

TMB was chosen as a chromogenic substrate for Fe^0@FeMn-NC nano-enzymes to evaluate the peroxidase-like activity of the nano-enzymes due to its ability to be catalytically oxidized by Fe^0@FeMn-NC nano-enzymes to a blue color product (OxTMB) in the presence of H_2O_2 (Fig. 4a). Compared to the addition of NC-900 only, Fe-NC, and

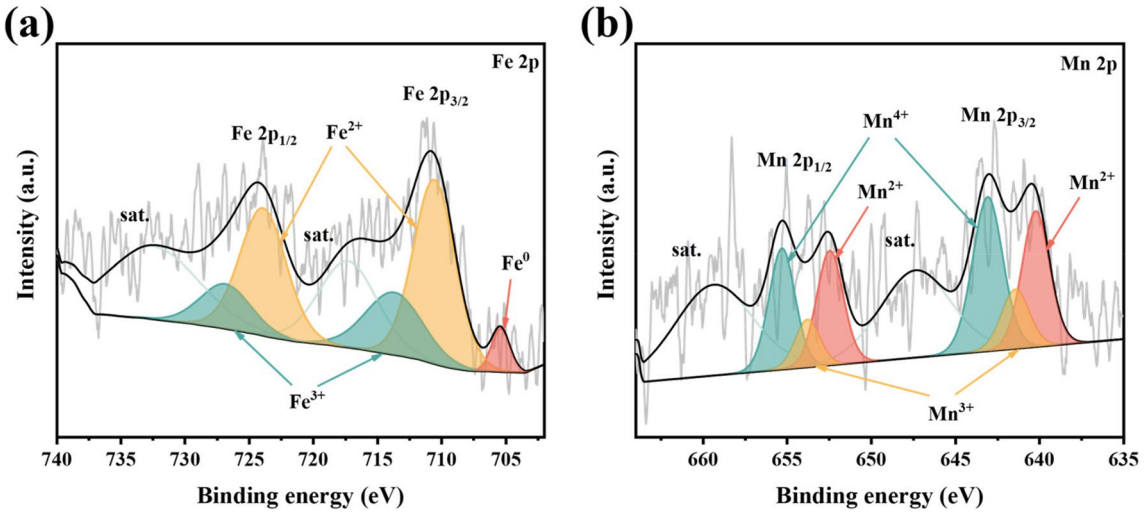

Fig. 3 XPS spectra of **a** Fe 2p and **b** Mn 2p for Fe^0@FeMn-NC

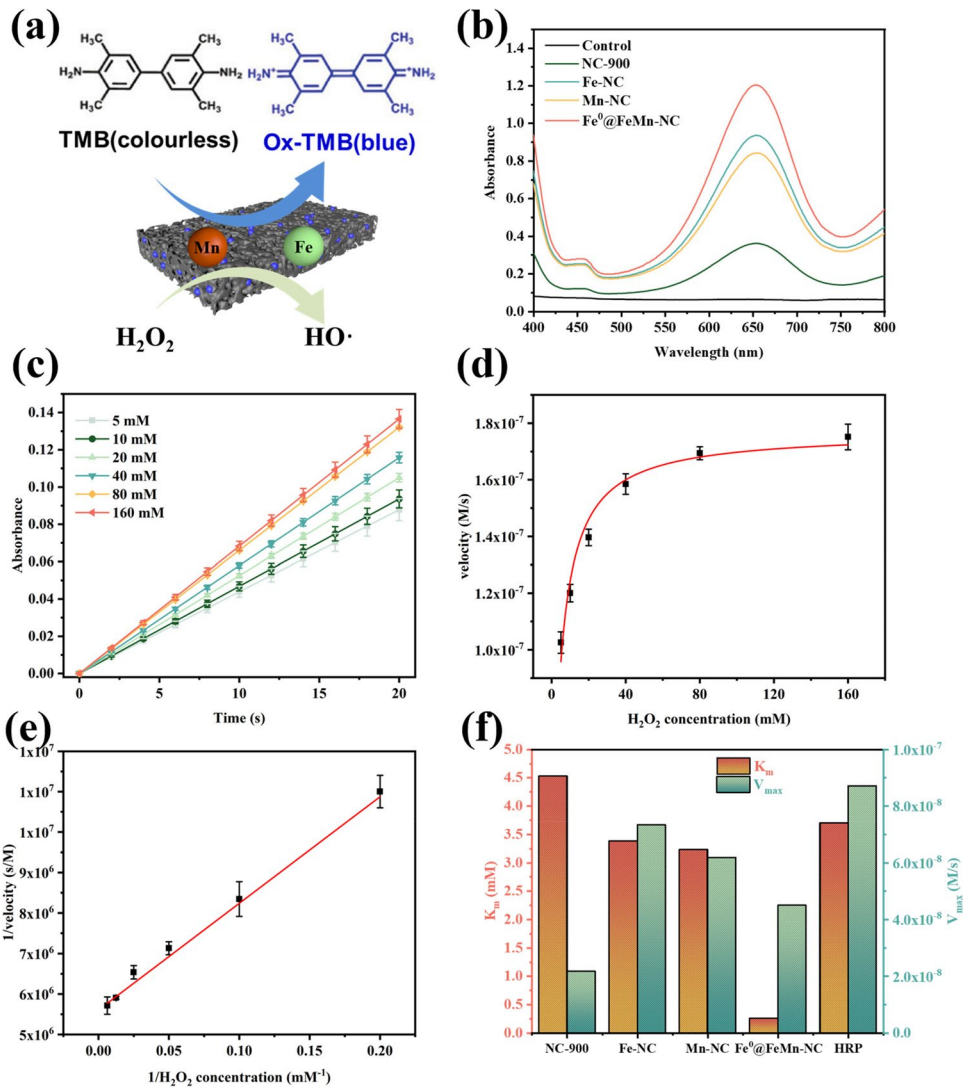

Fig. 4 **a** Oxidation of TMB by Fe^0@FeMn-NC peroxidase-like produces the blue product Ox-TMB; **b** UV-vis absorption spectra of NC-900, Fe-NC, Mn-NC, and Fe^0@FeMn-NC in the system with TMB + H_2O_2; steady-state kinetic assay of Fe^0@FeMn-NC nano-enzyme: **c** time-dependent absorption changes at 652 nm in the presence of different concentrations of H_2O_2; **d** the velocities were measured with different H_2O_2 concentrations; **e** double-reciprocal plots between velocity and H_2O_2 concentration; **f** K_m and V_{max} comparison of different nano-enzymes

Mn-NC, Fe^0@FeMn-NC had the maximum absorbance at 652 nm, indicating the highest peroxidase-like activity (Fig. 4b). It proved that there is a synergistic effect between Fe and Mn. When both are present together, they can effectively increase the peroxidase activity.

To quantitatively assess the peroxidase activity of NC-900, Fe-NC, Mn-NC, and Fe^0@FeMn-NC nano-enzymes, the Michaelis-Menten constants (K_m) and the maximum reaction rates (V_{max}) were determined using double-inverse plots of the initial reaction rates (Fig. 4c–e, Fig. S3, Fig. S4, and Fig. S5). As shown in Fig. 4f, the K_m values (3.38, 3.23, and 0.25 mM) of the three nano-enzymes were lower than those of HRP (3.7 mM (Gao et al. 2007)), except for NC-900 (K_m = 4.53 mM), when H_2O_2 was used as substrate. It indicates that Fe/Mn-doped nano-enzymes have more excellent affinity for H_2O_2 than HRP, and among them, Fe^0@FeMn-NC is the best. Most encouragingly, the newly synthesized Fe-Mn bimetallic peroxidase mimic in this study exhibited a higher affinity for H_2O_2 compared to other classes of peroxidized nano-enzymes previously reported (Fig. S6 and Table S2).

Catalytic degradation of 4-CP by Fe^0@FeMn-NCnano-enzymes

To demonstrate the actual catalytic performance of Fe^0@FeMn-NC nano-enzyme, 4-CP was selected as a target pollutant to test the degradation effect. We explored the factors affecting the degradation of 4-CP, such as nano-enzyme species, nano-enzyme dosing, pH, and H_2O_2 concentration. Figure 6a shows the removal efficiency of 4-CP in different reaction systems. Since all four materials have rich microporous structures, they showed excellent adsorption effects before the addition of H_2O_2 and basically reached the adsorption equilibrium after 30 min. The concentration of 4-CP in the Fe^0@FeMn-NC system decreased rapidly after the addition of H_2O_2. This system was able to remove 94.62% of 4-CP within 2 min, and the removal rate was as high as 98.91% after 30 min of oxidation. It indicates that Fe^0@FeMn-NC has a strong H_2O_2 activation ability and can accelerate the oxidative degradation of 4-CP by H_2O_2.

The effect of different Fe^0@FeMn-NC dosages on the removal efficiency of 4-CP is shown in Fig. 5b. Firstly, the removal efficiency of 4-CP increased with the increase of Fe^0@FeMn-NC concentration, from 62.65% at 5 mg/L to 98.91% at 40 mg/L. Subsequently, continuing to increase the dosage of Fe^0@FeMn-NC did not improve the removal of 4-CP. The removal rate of Fe^0@FeMn-NC at 80 mg/L decreased to 98.76% at 60 min, which showed a certain inhibitory effect on the degradation of 4-CP, suggesting that excessive Fe^0 would lead to the ineffective decomposition of H_2O_2.

It is well known that pH has a significant effect on the formation of hydroxyl radicals and the degradation process of pollutants in Fenton/Fenton-like systems (Masomboon et al. 2009; Wang et al. 2022). With similarity to the Fenton system, the Fe^0@FeMn-NC in this study had a higher degradation effect at low pH (3–6) (Fig. 5c), which can be attributed to the following factors: (1) low pH is favorable for the generation of ·OH (Kim et al. 2010); (2) it is beneficial to strengthen the catalytic oxidation ability of ·OH; and (3) facilitates the activation of Fe species (Xia et al. 2022).

In addition, the H_2O_2 concentration has a crucial effect on the degradation of 4-CP. In this study, the effect of different H_2O_2 concentrations on the degradation of 4-CP was investigated by varying the amount of H_2O_2 dosed in the system, and the results are shown in Fig. 5d. When the H_2O_2 concentration was 1 mM, the degradation of 4-CP by Fe^0@FeMn-NC was 90.11% at 60 min. With the increase of H_2O_2 concentration, the degradation efficiency of 4-CP gradually increased and reached a maximum of 98.91% at 10 mM. Subsequently, the final degradation efficiency no longer increased after the concentration continued to increase. This indicates that the dosage of H_2O_2 has reached the optimum at 10 mM, and due to the limitation of the number of active sites, it is difficult to decompose the excess H_2O_2 effectively, and then, the degradation efficiency cannot be improved.

Furthermore, the performances of different catalysts in the degradation of 4-CP reported in selected literature are summarized in Table 1. It is noteworthy that, in comparison with previous studies, Fe^0@FeMn-NC prepared by one-step pyrolytic reduction method in this study has excellent 4-CP degradation ability, and its performance is no less than that of conventional non-homogeneous catalysts. This fully demonstrates that our synthesized Fe^0@FeMn-NC is an excellent catalyst capable of efficiently degrading organic pollutants in wastewater.

Mechanistic studies

Toward revealing the internal mechanism of Fe^0@FeMn-NC nano-enzymatic catalysis, different radical burst experiments were designed according to the strong oxidizing radicals that may be generated during the classical H_2O_2-based advanced oxidation process, and the results are shown in Fig. S7a. Tert-Butanol (TBA), p-benzoquinone (PBQ), and furfuryl alcohol (FFA) were used as scavengers for •OH, $•O_2^-$ and $^1O_2$, respectively (Ma et al. 2021; Yun et al. 2018; Zhu et al. 2020). Firstly, the degradation rate of 4-CP decreased from 98.91 to 63.55% within 60 min with the addition of 50 mM TBA. The degradation rate further decreased to 60.25% when the concentration of TBA was increased to 100 mM. The degradation rate of 4-CP was likewise significantly inhibited by 50 mM FFA (degradation rate decreased to 69.72%). In contrast, the effect of PBQ on the removal of

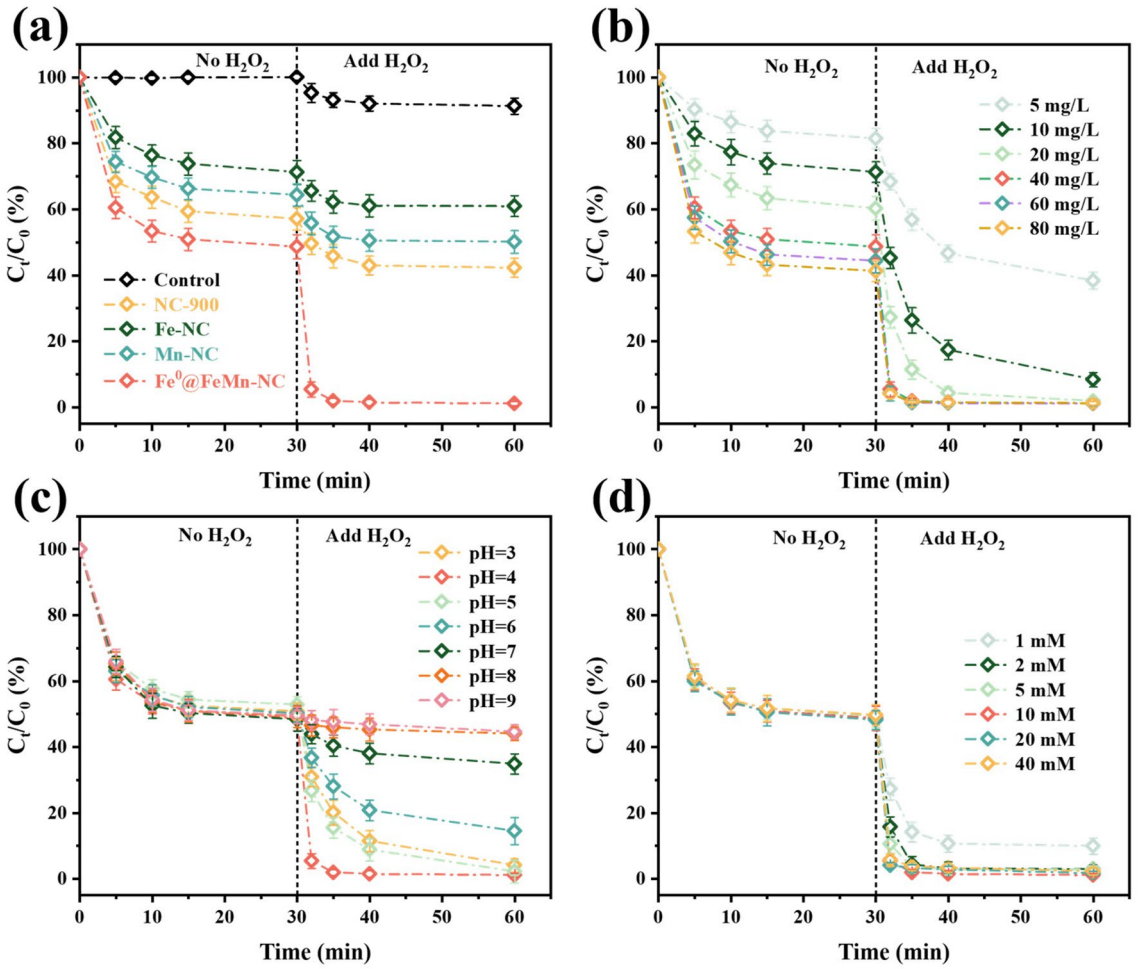

Fig. 5 Factors affecting the degradation of 4-CP: **a** type of nano-enzymes; **b** dosage of nano-enzymes; **c** pH; **d** H_2O_2 concentration. In addition to the condition to be controlled, other reaction conditions: pH = 4, [4-CP] = 100 mg/L, [nano-enzyme] = 40 mg/L, $[H_2O_2]$ = 10 mM, adsorption time = 30 min, reaction time = 30 min

Table 1 Comparison of different catalysts in the degradation of 4-CP

Catalyst	Reaction conditions	Degradation efficiency	Time (min)	Ref
HACO-P	[4-CP] = 2 g/L, $[H_2O_2]$ = 0.1 mM, [catalyst] = 3 g/L, pH_0 = 3.0	100%	120	(Wang et al. 2022)
MAC	[4-CP] = 100 mg/L, $[H_2O_2]$ = 20 mM, [catalyst] = 0.3 g/L, pH_0 = 3.0	92%	180	(Duan et al. 2020)
Fe_3O_4@Fe_3O_4/C	[4-CP] = 200 mg/L, $[H_2O_2]$ = 20 mM, [catalyst] = 0.5 g/L, pH_0 = 4.0	97%	180	(Zeng et al. 2014)
Fe-rich biochar	[4-CP] = 100 mg/L, $[H_2O_2]$ = 30 mM, [catalyst] = 2 g/L, pH_0 = 2.0	100%	120	(Gan et al. 2020)
Activated carbon/magnetite nano-catalyst	[4-CP] = 250 mg/L, $[H_2O_2]$ = 25.58 mM, [catalyst] = 2 g/L, pH_0 = 3.0	97.32%	78	(Haghmohammadi et al. 2023)
Fe^0@FeMn-NC	[4-CP] = 100 mg/L, $[H_2O_2]$ = 2 mM, [catalyst] = 0.04 g/L, pH_0 = 4.0	98.91%	30	This work

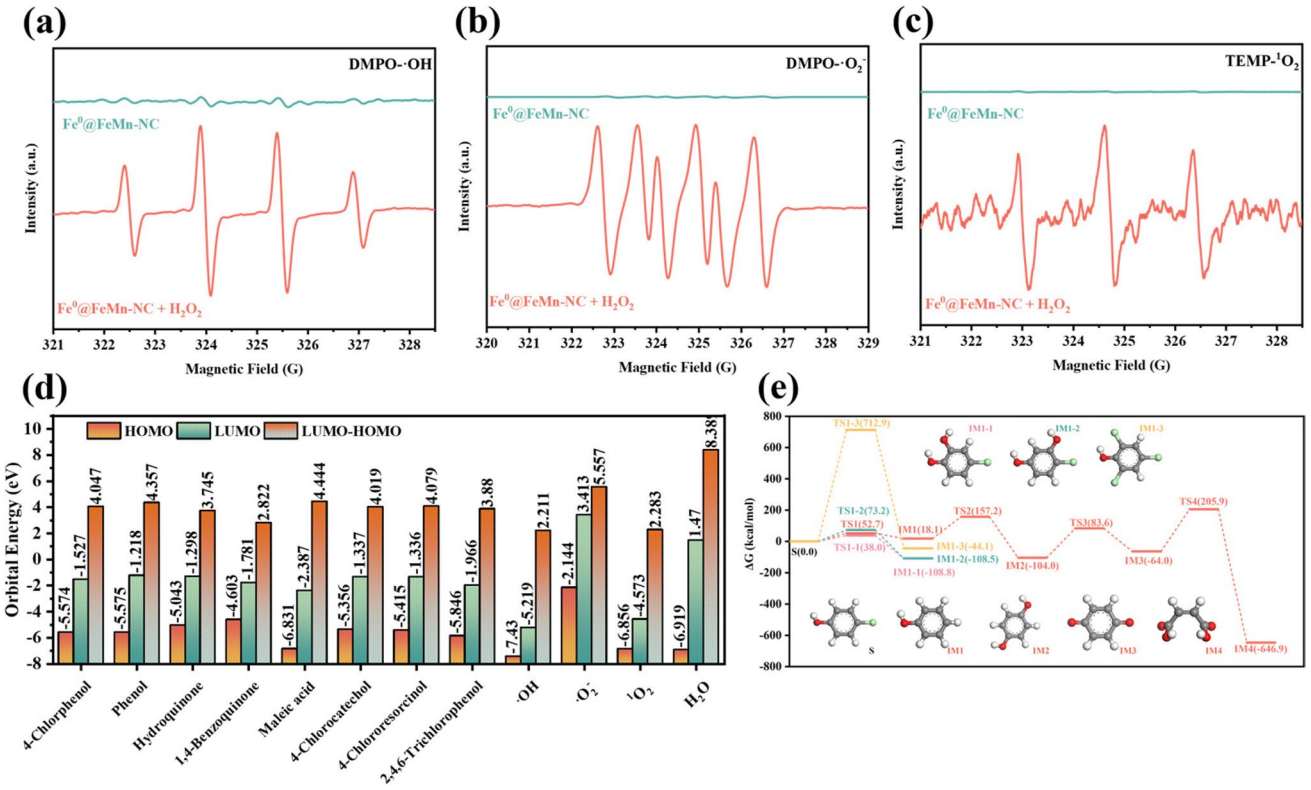

Fig. 6 EPR spectra of •OH (**a**) and $•O_2^-$ (**b**) with DMPO as trapping agent and $^1O_2$ (**c**) with TEMP as trapping agent in Fe^0@FeMn-NC/H_2O_2 system; **d** comparison of single-molecule orbital energy levels of 4-CP and its degradation intermediates (HOMO, LUMO, and LUMO-HOMO energy gaps); **e** the reaction barriers ΔG (kcal/mol) of 4-CP, its degradation intermediates, and transition states obtained by transition state search

4-CP was less pronounced. Fifty millimolar PBQ merely reduced the degradation of 4-CP to 78.69%. Finally, based on the inhibition effect of different quenchers on 4-CP degradation, we obtained the contribution of •OH, $•O_2^-$, and $^1O_2$ to the degradation of 4-CP (Fig. S7b). It can be seen that •OH and $^1O_2$ are the main ROS within the Fe^0@FeMn-NC/H_2O_2 system, and $•O_2^-$ is the minor one.

The role of •OH, $•O_2^-$, and $^1O_2$ in the system was further demonstrated by the determination of free radicals in the reaction by electron paramagnetic resonance spectroscopy. To the reaction system, 5,5-dimethyl-l-pyrrolidine N-oxide (DMPO) was added for the detection of •OH and $•O_2^-$ and 2,6,6-tetramethylpiperidine (TEMP) was used for the detection of $^1O_2$. The results are shown in Fig. 6a–c, where the signals of •OH, $•O_2^-$, and $^1O_2$ were detected. This further confirms that there are not only radical pathways of •OH and $•O_2^-$ but also non-radical pathways of $^1O_2$ during the degradation of 4-CP.

In this study, Fe^0 was introduced on the basis of the classical Fenton system (e.g., Eqs. (2)–(4)). Since Fe^0@FeMn-NC was added in solid form, a two-stage reaction was involved, starting with a non-homogeneous process of H_2O_2 on the surface of Fe^0@FeMn-NC, where Fe^0 transfers two electrons to the H_2O_2 to be oxidized to Fe^{2+} (Eq. (5)). Notably, competitive adsorption of 4-CP on the catalyst surface resulted in a decrease in the number of active sites exposed to the catalyst surface, thus prolonging the first stage of the reaction process. The second stage involves a rapid degradation process of the pollutant, mainly by Fe^{2+} catalyzing a homogeneous oxidation reaction on or near the catalyst surface. Strongly oxidizing •OH is rapidly produced in this phase.

Meanwhile, Fe^{2+} is regenerated from Fe^{3+} by reaction Eqs. (3) and (6), which promote the formation of •OH. However, Fe^0 not only promotes the reduction of Fe^{3+} on the catalyst surface but also generates H_2O_2 in situ in the presence of dissolved oxygen to further oxidize the pollutant (Eq. (7)). In addition, $^1O_2$ generated by disproportionation and auto-decomposition between free radicals contributes significantly to the degradation of 4-CP (Eqs. (8)–(9)). Manganese doping resulted in the appearance of a significant increase in the degradation efficiency of 4-CP. On the one hand, it is because similar to iron ions, Mn^{2+} can also participate in the chain reaction of free radicals in the catalytic system and can catalyze the decomposition of H_2O_2 to produce •OH (Eq. (10)). On the other hand, manganese atoms can make the iron atoms in the Fe-Mn binary oxides separate

and be reduced to zero-valent iron under high temperature environment, thus effectively improving the activation efficiency of H_2O_2. Eventually, 4-CP is co-oxidized by •OH, $•O_2^-$, and $^1O_2$ to produce various intermediates and eventually mineralized to CO_2 and H_2O (Eq. (11)).

$$H_2O_2 + Fe^{2+} \rightarrow Fe^{3+} + •OH + OH^- k = 40 - 80 M^{-1}s^{-1} \quad (2)$$

$$H_2O_2 + Fe^{3+} \rightarrow Fe^{2+} + HO_2• + H^+ k = 0.001 - 0.01 M^{-1}s^{-1} \quad (3)$$

$$HO_2• \leftrightarrow •O_2^- + H^+ \quad (4)$$

$$Fe^0 + H_2O_2 + 2H^+ \rightarrow Fe^{2+} + 2H_2O \quad (5)$$

$$2Fe^{3+} + Fe^0 \rightarrow 3Fe^{2+} \quad (6)$$

$$Fe^0 + O_2 + 2H^+ \rightarrow Fe^{2+} + H_2O_2 \quad (7)$$

$$•O_2^- + •OH \rightarrow OH^- + {}^1O_2 \quad (8)$$

$$•O_2^- + HO_2• \rightarrow {}^1O_2 + HO_2^- \quad (9)$$

$$H_2O_2 + Mn^{2+} \rightarrow Mn^{3+} + •OH + OH^- \quad (10)$$

$$•OH/•O_2^-/{}^1O_2 + 4 - CP \rightarrow \text{intermediate} + CO_2 + H_2O \quad (11)$$

Since Fe^0@FeMn-NC nano-enzymes have excellent catalytic degradation activity for 4-CP, it indicates that a large number of intermediate products are bound to be generated within this reaction system. And how to identify and characterize the intermediate products during the reaction process is crucial for exploring the degradation pathway of 4-CP. In this experiment, the intermediates during the degradation of 4-CP in the Fe^0@FeMn-NC/H_2O_2 system were analyzed by LC-MS and combined with the analysis of 4-CP degradation pathways by Liu et al. and Lei et al. (Hong et al. 2022; Lei et al. 2021). It was initially deduced that the intermediates for the degradation of 4-CP may include phenol ($m/z = 96$), benzoquinone ($m/z = 108$), hydroquinone ($m/z = 110$), maleic acid ($m/z = 116$), malic acid ($m/z = 116$), 4-chlorocatechol ($m/z = 144$), and 2,4,6-trichlorophenol ($m/z = 195$), as shown in Fig. S8.

To successfully predict the interaction modes during the degradation of 4-CP, we calculated the highest occupied molecular orbital energy (HOMO), the lowest unoccupied molecular orbital energy (LUMO), and the LUMO-HOMO energy gap of the ground state (S) and the degradation intermediate state (IM) of 4-CP. Besides, the transition state (TS) energy barriers of the corresponding reactions were calculated, and the results are shown in Fig. 6d, e. Molecules with high HOMO energies favor reactions with electrophilic molecules, while molecules with lower LUMO energies show affinity for nucleophilic reagents (Liu et al. 2014). Thus, •OH (− 5.219 eV) with the lowest LUMO orbital energy is able to easily replace the hydrogen in the neighboring and interstitial positions of the hydroxyl group on the benzene ring by electrophilic addition reactions. This results in the conversion of 4-CP to 4-chlorocatechol (IM1-1) and 4-chlororesorcinol (IM1-2). The lower LUMO orbital energy of $^1O_2$ (− 4.573 eV) can effectively dechlorinate 4-CP and generate hydroquinone (IM2) through the electrophilic addition reaction of •OH. In turn, p-chlorophenol in solution is subjected to the action of the dechlorinated chlorine radicals in the system to produce trace amounts of 2,4,6-trichlorophenol (IM1-3) with a reaction energy barrier of 712.9 kcal/mol. unstable hydroquinone (− 5.043 eV for HOMO) is readily oxidized to p-benzoquinone (IM3). Immediately thereafter, due to the lower LUMO-HOMO energy gap (2.822 eV), p-benzoquinone is highly susceptible to oxidative ring-opening by electrophilic •OH and $^1O_2$ to form, for example, maleic acid and malic acid, and these small-molecule acids are able to be further mineralized ultimately to CO_2 and H_2O. In summary, the degradation process of 4-CP in the Fe^0@FeMn-NC/H_2O_2 system was summarized in Fig. S9.

Repeatability and stability studies

As to evaluate the stability and TOC removal rate of Fe^0@FeMn-NC nano enzymes, the degradation rates of 4-CP and TOC were determined under five cycling experiments, and the results are shown in Fig. S10. The 4-CP degradation rates in the five cycling experiments were maintained above 90%, while the TOC removal rates were maintained above 40%. This indicates that the Fe^0@FeMn-NC nano-enzyme still has good catalytic activity under repeated use. In addition, the ion leaching of Fe-NC, Mn-NC, and Fe^0@FeMn-NC in five-cycle experiments was compared (Fig. 7a, b), and the results showed that the doping of Fe with Mn could reduce the leaching of metal ions, and it was gradually decreased in several cycles. The above results further proved that the nano-enzymes have good stability and environmental safety.

Degradation of multiple pollutants and treatment of actual wastewater

The degradation efficiency of the Fe^0@FeMn-NC/H_2O_2 system for a variety of phenolic pollutants and its application in real wastewater were investigated. As shown in Fig. 7c, Fe^0@FeMn-NC exhibited high adsorption rates for 4-CP, 4-NP, BPA, PCM, and Phenol. With the addition of H_2O_2 after 30 min of adsorption equilibrium, the final degradation

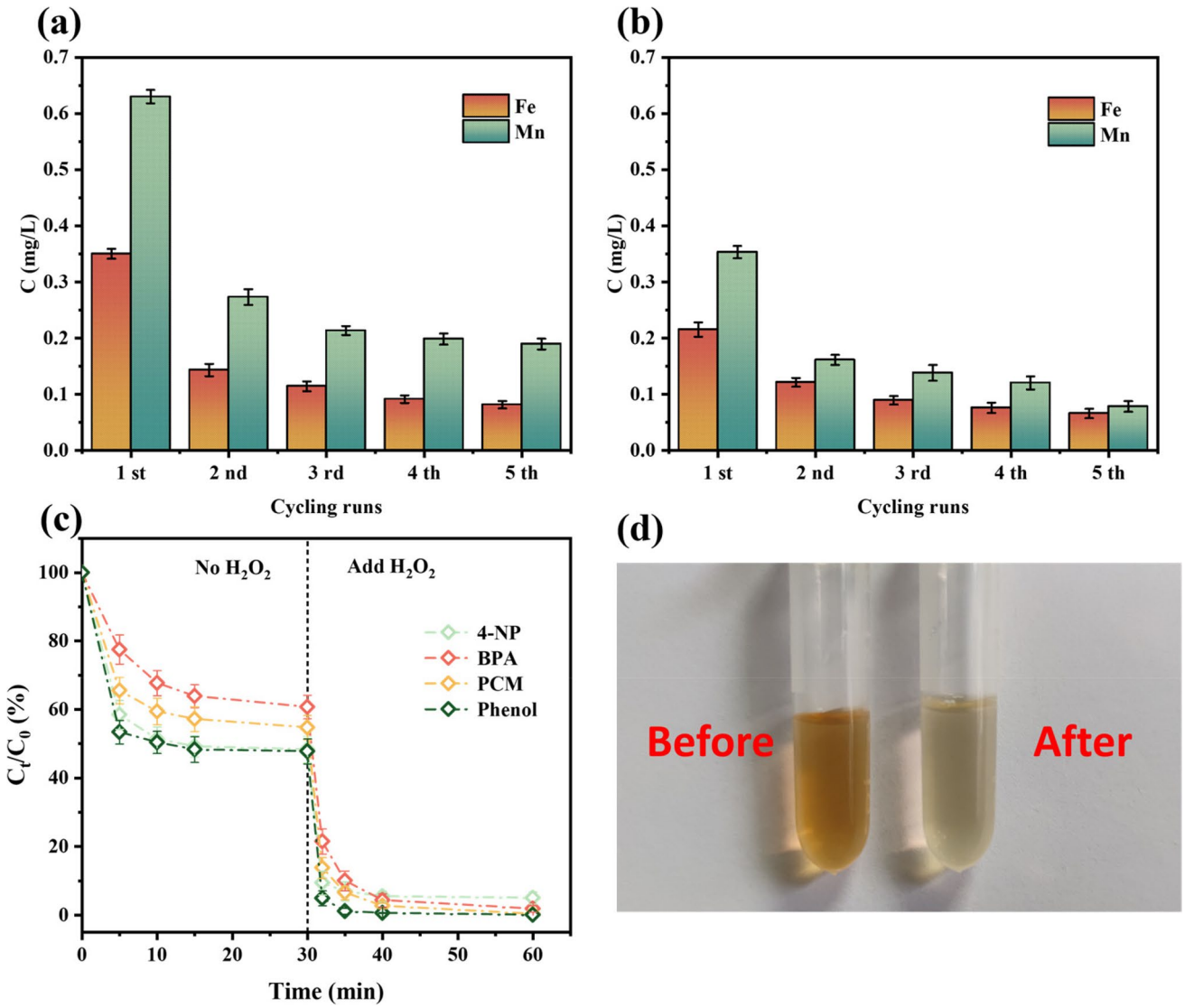

Fig. 7 Fe and Mn leaching concentrations of Fe-NC, Mn-NC (**a**) and Fe^0@FeMn-NC (**b**) during degradation of 4-CP (100 mg/L); **c** effects of Fe^0@FeMn-NC/H_2O_2 system on the degradation of 4-NP, BPA, PCM, and Phenol (10 mg/L); **d** changes in raw water in the workshop of a chemical plant before and after the reaction. Reaction conditions: pH = 4, [nano-enzyme] = 40 mg/L, [H_2O_2] = 10 mM, adsorption time = 30 min, reaction time = 30 min

rates of 4-NP, BPA, PCM, and Phenol were 95.04%, 98.21%, 99.73%, and 100%, respectively. It shows that the Fe^0@FeMn-NC/H_2O_2 system has the potential to treat a wide range of phenolic pollutants. Subsequently, raw workshop water from a chemical plant was used as the target effluent to study the degradation effect of the Fe^0@FeMn-NC/H_2O_2 system in a real wastewater environment (Table S3 and Fig. 7d). Firstly, its initial indicators were determined, and 4-CP, 4-NP, BPA, PCM, and Phenol were detected in this wastewater. Secondly, the pH was adjusted to 4.0, and Fe^0@FeMn-NC and H_2O_2 were successively added to it. Eventually, after 1 h of reaction, the removal of 4-CP, 4-NP, BPA, PCM, and Phenol reached 90.94%, 87.70%, 85.50%, 77.47%, and 93.98%, respectively. In addition, the indexes of turbidity and COD also decreased by 69.92% and 56.70%. This study demonstrates that Fe^0@FeMn-NC is a promising material for the treatment of high concentration organic wastewater.

Conclusion

In this study, an Fe^0-loaded Fe-Mn bimetallic peroxidase mimetic (Fe^0@FeMn-NC) was successfully prepared by a simple one-step thermal reduction method with Fe and Mn co-doping. Fe and Mn exist in the valence states of Fe^{3+}/

Fe^{2+}/Fe^0 and $Mn^{4+}/Mn^{3+}/Mn^{2+}$, which act as the key active sites catalyzing the decomposition of H_2O_2 to produce •OH and $•O_2^-$, as well as $^1O_2$, for the degradation and even mineralization of 4-CP. Among them, the role of Fe^0 should not be neglected, which promptly replenishes the constantly consumed Fe^{2+} in the reaction and brings in a large number of additional electrons. This avoids the ineffective decomposition of H_2O_2 due to the use of H_2O_2 as an electron donor during the reduction reaction of Fe^{3+} to Fe^{2+} and Mn^{3+} to Mn^{2+}. The degradation process of 4-CP, whose intermediates are mainly p-chloro-catechol, p-chloro resorcinol, and p-benzoquinone, was reasonably hypothesized based on the results of LC-MS detection and combined with theoretical calculations. The Fe^0@FeMn-NC/H_2O_2 system also showed high degradation efficiency for simulated wastewater containing multiple phenolic pollutants as well as real chemical plant wastewater. The successful application of Fe^0-loaded Fe^0@FeMn-NC nano-enzyme in the degradation of 4-CP presented in this work provides some insights and methods for the application of peroxidase-like enzymes in the degradation of organic pollutants.

Supplementary information The online version contains supplementary material available at https://doi.org/10.1007/s11356-023-31754-4.

Author contribution XL: conceptualization, methodology, validation, formal analysis, investigation, software, visualization, and writing—original draft. HL: methodology and investigation. ZL: investigation. MC: methodology. KC: writing—review and editing. ZG: writing—review and editing. ZD: writing—review and editing. BW: writing—review and editing. XC: conceptualization, supervision, project administration, funding acquisition, investigation, and writing—review and editing.

Funding The authors acknowledge the financial support from the Key Science and Technology Projects of Anhui Province (202003a07020004) and National Key R&D Program of China (2019YFC0408500).

Data availability All data generated or analyzed during this study are included in this published article and its supplementary information files.

Declarations

Ethics approval and consent to participate Not applicable.

Consent for publication All the authors listed have approved the manuscript that is enclosed.

Competing interests The authors declare no competing interests.

References

Ananthoju B, Biroju RK, Theis W, Dryfe RAW (2019) Controlled electrodeposition of gold on graphene: maximization of the defect-enhanced raman scattering response. Small 15(48):1901555. https://doi.org/10.1002/smll.201901555

Baye AF, Nguyen HT, Kim H (2023) Fe^0/Fe_3C-assisted Fe_3O_4 redox sites as robust peroxidase mimics for colorimetric detection of H_2O_2. Sens Actuators B-Chem 377:133097. https://doi.org/10.1016/j.snb.2022.133097

Cai M, Zhang Y, Dong C, Wu W, Wang Q, Song Z, Shi Y, Wu L, Jin M, Dionysiou DD, Wei Z (2021) Manganese doped iron-carbon composite for synergistic persulfate activation: reactivity, stability, and mechanism. J Hazard Mater 405:124228. https://doi.org/10.1016/j.jhazmat.2020.124228

Chen Q, Zhang X, Li S, Tan J, Xu C, Huang Y (2020) MOF-derived Co_3O_4@Co-Fe oxide double-shelled nanocages as multi-functional specific peroxidase-like nanozyme catalysts for chemo/biosensing and dye degradation. Chem Eng J 395:125130. https://doi.org/10.1016/j.cej.2020.125130

Czaplicka M (2004) Sources and transformations of chlorophenols in the natural environment. Sci Total Environ 322(1–3):21–39. https://doi.org/10.1016/j.scitotenv.2003.09.015

Darabdhara G, Das MR (2019) Dual responsive magnetic Au@Ni nanostructures loaded reduced graphene oxide sheets for colorimetric detection and photocatalytic degradation of toxic phenolic compounds. J Hazard Mater 368:365–377. https://doi.org/10.1016/j.jhazmat.2019.01.010

Delley B (1990) An all-electron numerical method for solving the local density functional for polyatomic molecules. J Chem Phys 92(1):508–517. https://doi.org/10.1063/1.458452

Delley B (2000) From molecules to solids with the $DMol^3$a pproach. J Chem Phys 113(18):7756–7764. https://doi.org/10.1063/1.1316015

Deng Y, Dong Y, Wang G, Sun K, Shi X, Zheng L, Li X, Liao S (2017) Well-defined ZIF-derived Fe-N codoped carbon nanoframes as efficient oxygen reduction catalysts. ACS Appl Mater Interfaces 9(11):9699–9709. https://doi.org/10.1021/acsami.6b16851

Ding Y, Cui K, Guo Z, Cui M, Chen Y (2021) Manganese peroxidase mediated oxidation of sulfamethoxazole: integrating the computational analysis to reveal the reaction kinetics, mechanistic insights, and oxidation pathway. J Hazard Mater 415:125719. https://doi.org/10.1016/j.jhazmat.2021.125719

Du J, Xiao G, Xi Y, Zhu X, Su F, Kim SH (2020) Periodate activation with manganese oxides for sulfanilamide degradation. Water Res 169:115278. https://doi.org/10.1016/j.watres.2019.115278

Duan Z, Zhang W, Lu M, Shao Z, Huang W, Li J, Li Y, Mo J, Li Y, Chen C (2020) Magnetic Fe_3O_4/activated carbon for combined adsorption and Fenton oxidation of 4-chlorophenol. Carbon 167:351–363. https://doi.org/10.1016/j.carbon.2020.05.106

Duan L, Liu X, Zhang H, Liu F, Liu X, Zhang X, Dong L (2022) A novel way for hydroxyl radicals generation: biochar-supported zero-valent iron composite activates oxygen to generate hydroxyl radicals. J Environ Chem Eng 10(4):108132. https://doi.org/10.1016/j.jece.2022.108132

Feng J, Yang X, Du T, Zhang L, Zhang P, Zhuo J, Luo L, Sun H, Han Y, Liu L, Shen Y, Wang J, Zhang W (2023) Transition metal high-entropy nanozyme: multi-site orbital coupling modulated high-efficiency peroxidase mimics. Adv Sci 10(33):2303078. https://doi.org/10.1002/advs.202303078

Gan Q, Hou H, Liang S, Qiu J, Tao S, Yang L, Yu W, Xiao K, Liu B, Hu J, Wang Y, Yang J (2020) Sludge-derived biochar with multivalent iron as an efficient Fenton catalyst for degradation of 4-Chlorophenol. Sci Total Environ 725:138299. https://doi.org/10.1016/j.scitotenv.2020.138299

Gao L, Zhuang J, Nie L, Zhang J, Zhang Y, Gu N, Wang T, Feng J, Yang D, Perrett S, Yan X (2007) Intrinsic peroxidase-like activity of ferromagnetic nanoparticles. Nat Nanotechnol 2(9):577–583. https://doi.org/10.1038/nnano.2007.260

Gong L, Qiu X, Tratnyek PG, Liu C, He F (2021) FeNX(C)-coated microscale zero-valent iron for fast and stable trichloroethylene dechlorination in both acidic and basic pH conditions. Environ Sci Technol 55(8):5393–5402. https://doi.org/10.1021/acs.est.0c08176

Haghmohammadi M, Sajjadi N, Beni AA, Hakimzadeh SM, Nezarat A, Asl SD (2023) Synthesis of activated carbon/magnetite nanocatalyst for sono-Fenton-like degradation process of 4-chlorophenol in an ultrasonic reactor and optimization using response surface method. J Water Process Eng 55:104216. https://doi.org/10.1016/j.jwpe.2023.104216

He L, Li H, Wang J, Gao Q, Li X (2022) Peroxymonosulfate activation by Co-doped magnetic Mn_3O_4 for degradation of oxytetracycline in water. Environ Sci Pollut Res 29(26):39249–39265. https://doi.org/10.1007/s11356-022-18929-1

He T, Pan X, Zhou W, Ding H, Liu M, Xiang M, Lou Q, Han L, Zhang Y, Wu Y, Chen Y (2023) Construction of high-content α-iron on zero-valent iron @ biochar composite for the ultra-efficient removal of oxytetracycline hydrochloride: a key step of ammonium bicarbonate pretreatment. Sep Purif Technol 323:124378. https://doi.org/10.1016/j.seppur.2023.124378

He Y, Qin H, Wang Z, Wang H, Zhu Y, Zhou C, Zeng Y, Li Y, Xu P, Zeng G (2024) Fe-Mn oxycarbide anchored on N-doped carbon for enhanced Fenton-like catalysis: importance of high-valent metal-oxo species and singlet oxygen. Appli Catal B-Environ 340:123204. https://doi.org/10.1016/j.apcatb.2023.123204

Hong P, Zhang K, He J, Li Y, Wu Z, Xie C, Liu J, Kong L (2022) Selenization governs the intrinsic activity of copper-cobalt complexes for enhanced non-radical Fenton-like oxidation toward organic contaminants. J Hazard Mater 435:128958. https://doi.org/10.1016/j.jhazmat.2022.128958

Hu E, Zhang Y, Wu S, Wu J, Liang L, He F (2017) Role of dissolved Mn(III) in transformation of organic contaminants: non-oxidative versus oxidative mechanisms. Water Res 111:234–243. https://doi.org/10.1016/j.watres.2017.01.013

Hu H, Miao K, Luo X, Guo S, Yuan X, Pei F, Qian H, Feng G (2021) Efficient Fenton-like treatment of high-concentration chlorophenol wastewater catalysed by Cu-Doped SBA-15 mesoporous silica. J Clean Prod 318:128632. https://doi.org/10.1016/j.jclepro.2021.128632

Huang S, Qiao Z, Sun P, Qiao K, Pei K, Yang L, Xu H, Wang S, Huang Y, Yan Y, Cao D (2022) The strain induced synergistic catalysis of FeN_4 and MnN_3 dual-site catalysts for oxygen reduction in proton-/anion- exchange membrane fuel cells. Appl Catal B-Environ 317:121770. https://doi.org/10.1016/j.apcatb.2022.121770

Huang H, Geng W, Wu X, Zhang Y, Xie L, Ma T, Cheng C (2023) Spiky artificial peroxidases with V−O−Fe pair sites for combating antibiotic-resistant pathogens. Angew Chem Int Ed e202310811. https://doi.org/10.1002/anie.202310811

Jiang G, Wang Z, Zong S, Yang K, Zhu K, Cui Y (2021) Peroxidase-like recyclable SERS probe for the detection and elimination of cationic dyes in pond waterY. J Hazard Mater 408:124426. https://doi.org/10.1016/j.jhazmat.2020.124426

Jiao L, Xu W, Zhang Y, Wu Y, Gu W, Ge X, Chen B, Zhu C, Guo S (2020) Boron-doped Fe-N-C single-atom nanozymes specifically boost peroxidase-like activity. Nano Today 35:100971. https://doi.org/10.1016/j.nantod.2020.100971

Kim JY, Lee C, Sedlak DL, Yoon J, Nelson KL (2010) Inactivation of MS_2 coliphage by Fenton's reagent. Water Res 44(8):2647–2653. https://doi.org/10.1016/j.watres.2010.01.025

Lai Q, Zhao Y, Liang Y, He J, Chen J (2016) In situ confinement pyrolysis transformation of ZIF-8 to nitrogen-enriched meso-microporous carbon frameworks for oxygen reduction. Adv Func Mater 26(45):8334–8344. https://doi.org/10.1002/adfm.201603607

Lei M, Gao Q, Zhou K, Gogoi P, Liu J, Wang J, Song H, Wang S, Liu X (2021) Catalytic degradation and mineralization mechanism of 4-chlorophenol oxidized by phosphomolybdic acid/H_2O_2. Sep Purif Technol 257:117933. https://doi.org/10.1016/j.seppur.2020.117933

Liang F, Liu Z, Jiang X, Li J, Xiao K, Xu W, Chen X, Liang J, Lin Z, Li M, Wu X, Wang H (2023) NaOH-modified biochar supported Fe/Mn bimetallic composites as efficient peroxymonosulfate activator for enhance tetracycline removal. Chem Eng J 454:139949. https://doi.org/10.1016/j.cej.2022.139949

Liang J, Zhou RF, Chen XM, Tang YH, Qiao SZ (2014) Fe-N decorated hybrids of CNTs grown on hierarchically porous carbon for high-performance oxygen reduction. Adv Mater 26(35):6074-+. https://doi.org/10.1002/adma.201401848

Lin J, Sun M, Liu X, Chen Z (2017) Functional kaolin supported nanoscale zero-valent iron as a Fenton-like catalyst for the degradation of Direct Black G. Chemosphere 184:664–672. https://doi.org/10.1016/j.chemosphere.2017.06.038

Liu H, Chen Q, Zhang S, Li X (2014) Relationship of mineralization of amino naphthalene sulfonic acids by Fenton oxidation and frontier molecular orbital energies. Chem Eng J 247:275–282. https://doi.org/10.1016/j.cej.2014.03.019

Liu J, Ghanizadeh H, Li X, An L, Qiu Y, Zhang Y, Chen X, Wang A (2022) Facile synthesis of core\shell Fe_3O_4@mSiO_2(Hb) and its application for organic wastewater treatment. Environ Res 203:111796. https://doi.org/10.1016/j.envres.2021.111796

Liu B, Wang Z, Wei T, Liu Z, Li J (2023a) Bimetallic FeMn-N nanoparticles as nanocatalyst with dual enzyme-mimic activities for simultaneous colorimetric detection and degradation of hydroquinone. J Environ Chem Eng 11(3):110186. https://doi.org/10.1016/j.jece.2023.110186

Liu C, Zheng J, Zhang B, Zhong X, Wang W, Li Z (2023b) BSA-$Cu_3(PO_4)_2$ hybrid nanoflower-an efficient and low-cost nanoenzyme for decolorization of organic pollutants. Anal Bioanal Chem 415(9):1687–1698. https://doi.org/10.1007/s00216-023-04563-4

Lv X, Foda MF, He J, Zhou J, Cai J (2023) Robust and facile label-free colorimetric aptasensor for ochratoxin A detection using aptamer-enhanced oxidase-like activity of MnO_2 nanoflowers. Food Chem 401:134144. https://doi.org/10.1016/j.foodchem.2022.134144

Ma J, Zhang S, Duan X, Wang Y, Wu D, Pang J, Wang X, Wang S (2021) Catalytic oxidation of sulfachloropyridazine by MnO_2: effects of crystalline phase and peroxide oxidants. Chemosphere 267:129287. https://doi.org/10.1016/j.chemosphere.2020.129287

Mao YW, Zhang J, Zhang R, Li JQ, Wang AJ, Zhou XC, Feng JJ (2023) N-doped carbon nanotubes supported Fe-Mn dual-single-atoms nanozyme with synergistically enhanced peroxidase activity for sensitive colorimetric detection of acetylcholinesterase and its inhibitor. Anal Chem 95(22):8640–8648. https://doi.org/10.1021/acs.analchem.3c01070

Martins MBMS, Correa GA, Moniz T, Medforth CJ, de Castro B, Rebelo SLH (2023) Nanostructured binuclear Fe(III) and Mn(III) porphyrin materials: tuning the mimics of catalase and peroxidase activity. J Catal 419:125–136. https://doi.org/10.1016/j.jcat.2023.02.001

Masomboon N, Ratanatamskul C, Lu MC (2009) Chemical oxidation of 2,6-dimethylaniline in the Fenton process. Environ Sci Technol 43(22):8629–8634. https://doi.org/10.1021/es802274h

Meng Y, Zhao K, Zhang Z, Gao P, Yuan J, Cai T, Tong Q, Huang G, He D (2020) Effects of crystal structure on the activity of MnO_2 nanorods oxidase mimics. Nano Res 13(3):709–718. https://doi.org/10.1007/s12274-020-2680-5

Mishra P, Lee J, Kumar D, Lauro RO, Costa N, Pathania D, Kumar S, Lee J, Singh L (2022) Engineered nanoenzymes with multifunctional properties for next-generation biological and environmental applications. Adv Func Mater 32(8):2108650. https://doi.org/10.1002/adfm.202108650

Perdew JP, Burke K, Ernzerhof M (1996) Generalized gradient approximation made simple. Phys Rev Lett 77(18):3865–3868. https://doi.org/10.1103/PhysRevLett.77.3865

Qu M, Qin G, Fan J, Du A, Sun Q (2021) Theoretical insights into the performance of single and double transition metal atoms doped on N-graphenes for N_2 electroreduction. Appl Surf Sci 537:148012. https://doi.org/10.1016/j.apsuse.2020.148012

Sun M, He M, Jiang S, Wang Y, Wang X, Liu T, Song C, Wang S, Rao H, Lu Z (2021) Multi-enzyme activity of three layers FeOx@ZnMnFeOy@Fe-Mn organogel for colorimetric detection of antioxidants and norfloxacin with smartphone. Chem Eng J 425:131823. https://doi.org/10.1016/j.cej.2021.131823

Tang C, Fang T, Chen S, Zhang D, Yin J, Wang H (2023) Citrate-functionalized osmium nanoparticles with peroxidase-like specific activity for highly efficient degradation of phenolic pollutants. Chem Eng J 464:142726. https://doi.org/10.1016/j.cej.2023.142726

Villaluz FDA, de Luna MDG, Colades JI, Garcia-Segura S, Lu MC (2019) Removal of 4-chlorophenol by visible-light photocatalysis using ammonium iron(II) sulfate-doped nano-titania. Process Saf Environ Prot 125:121–128. https://doi.org/10.1016/j.psep.2019.03.001

Wan K, Jiang B, Tan T, Wang H, Liang M (2022) Surface-mediated production of complexed center dot ·OH radicals and Fe=O species as a mechanism for iron oxide peroxidase-like nanozymes. Small 18(50):2204372. https://doi.org/10.1002/smll.202204372

Wang L, Chen Y (2020) Luminescence-sensing Tb-MOF nanozyme for the detection and degradation of estrogen endocrine disruptors. ACS Appl Mater Interfaces 12(7):8351–8358. https://doi.org/10.1021/acsami.9b22537

Wang X, Nan Z (2020) Highly efficient Fenton-like catalyst Fe-g-C_3N_4 porous nanosheets formation and catalytic mechanism. Sep Purif Technol 233:116023. https://doi.org/10.1016/j.seppur.2019.116023

Wang B, Zou J, Shen X, Yang Y, Hu G, Li W, Peng Z, Banham D, Dong A, Zhao D (2019) Nanocrystal supracrystal-derived atomically dispersed Mn-Fe catalysts with enhanced oxygen reduction activity. Nano Energy 63:103851. https://doi.org/10.1016/j.nanoen.2019.06.047

Wang Y, Wang H, Wang L, Cai B, Chen H (2022) Removal of high-concentration 4-Chlorophenol (4-CP) in wastewater using carbon-based heterogeneous catalytic oxidation: performance and mechanism. J Clean Prod 346:131176. https://doi.org/10.1016/j.jclepro.2022.131176

Wei S, Sun Y, Qiu YZ, Li A, Chiang CY, Xiao H, Qian J, Li Y (2023) Self-carbon-thermal-reduction strategy for boosting the Fenton-like activity of single Fe-N_4 sites by carbon-defect engineering. Nat Commun 14(1):7549–7549. https://doi.org/10.1038/s41467-023-43040-5

Xia Q, Zhang D, Yao Z, Jiang Z (2022) Revealing the enhancing mechanisms of Fe-Cu bimetallic catalysts for the Fenton-like degradation of phenol. Chemosphere 289:133195. https://doi.org/10.1016/j.chemosphere.2021.133195

Xing N, Lyu Y, Yang J, Zhang X, Han Y, Zhao W, Ng DHL, Li J (2022) Motion-based phenol detection and degradation using 3D hierarchical AA-NiMn-CLDHs@HNTs-Ag nanomotors. Environ Sci-Nano 9(8):2815–2826. https://doi.org/10.1039/d2en00322h

Xu L, He Z, Wei X, Shang Y, Shi J, Jin X, Bai X, Shi X, Jin P (2023a) Facile-prepared Fe/Mn co-doped biochar is an efficient catalyst for mediating the degradation of aqueous ibuprofen via catalytic ozonation. Chem Eng J 461:142028. https://doi.org/10.1016/j.cej.2023.142028

Xu Z, Sun M, Xu X, Cao X, Ippolito JA, Mohanty SK, Ni B-J, Xu S, Tsang DCW (2023b) Electron donation of Fe-Mn biochar for chromium(VI) immobilization: key roles of embedded zero-valent iron clusters within iron-manganese oxide. J Hazard Mater 456:131632. https://doi.org/10.1016/j.jhazmat.2023.131632

Yamashita T, Hayes P (2008) Analysis of XPS spectra of Fe^{2+} and Fe^{3+} ions in oxide materials. Appl Surf Sci 254(8):2441–2449. https://doi.org/10.1016/j.apsusc.2007.09.063

Yang H, Xue W, Liu M, Yu K, Yu W (2020) Carbon doped Fe_3O_4 peroxidase-like nanozyme for mitigating the membrane fouling by NOM at neutral pH. Water Res 174:115637. https://doi.org/10.1016/j.watres.2020.115637

Yun ET, Lee JH, Kim J, Park HD, Lee J (2018) Identifying the non-radical mechanism in the peroxymonosulfate activation process: singlet oxygenation versus mediated electron transfer. Environ Sci Technol 52(12):7032–7042. https://doi.org/10.1021/acs.est.8b00959

Zeng T, Zhang X, Wang S, Ma Y, Niu H, Cai Y (2014) Assembly of a nanoreactor system with confined magnetite core and shell for enhanced Fenton-like catalysis. Chem –Eur J 20(21):6474–6481. https://doi.org/10.1002/chem.201304221

Zhang WH, Quan X, Zhang ZY (2007) Catalytic reductive dechlorination of p-chlorophenol in water using Ni/Fe nanoscale particles. J Environ Sci 19(3):362–366. https://doi.org/10.1016/S1001-0742(07)60060-6

Zhang M, Wu D, Ye Y, Wu L, Yao Z, Ma X, Wang L, Zhang Z, Xiang S (2018) Thermal conversion of MOF@MOF: synthesis of an N-doped carbon material with excellent ORR performance. ChemPlusChem 83(11):1044–1051. https://doi.org/10.1002/cplu.201800392

Zhang L, Liu Z, Deng Q, Sang Y, Dong K, Ren J, Qu X (2021) Nature-inspired construction of MOF@COF nanozyme with active sites in tailored microenvironment and pseudopodia-like surface for enhanced bacterial inhibition. Angew Chem Int Ed 60(7):3469–3474. https://doi.org/10.1002/anie.202012487

Zhang C, Zhang X, Ye Y, Ni P, Chen C, Liu W, Wang B, Jiang Y, Lu Y (2022) Manganese-doped iron coordination polymer nanoparticles with enhanced peroxidase-like activity for colorimetric detection of antioxidants. Analyst 147(2):238–246. https://doi.org/10.1039/d1an01953h

Zhu W, Li Y, Dai L, Li J, Li X, Li W, Duan T, Lei J, Chen T (2018) Bioassembly of fungal hyphae/carbon nanotubes composite as a versatile adsorbent for water pollution control. Chem Eng J 339:214–222. https://doi.org/10.1016/j.cej.2018.01.134

Zhu MP, Yang JCE, Duan X, Zhang DD, Wang S, Yuan B, Fu ML (2020) Interfacial $CoAl_2O_4$ from ZIF-67@γ-Al_2O_3 pellets toward catalytic activation of peroxymonosulfate for metronidazole removal. Chem Eng J 397:125339. https://doi.org/10.1016/j.cej.2020.125339